This is the author's version of the work. It is posted here by permission of the AAAS for personal use, not for redistribution. The definitive version was published in Science vol. 371, 26 Feb 2021, 10.1126/science.aba1111

arXiv:2006.04833v1 [astro-ph.SR] 8 Jun 2020

Constraining the Rapid Neutron-Capture Process with Meteoritic ^{129}I and ^{247}Cm

Benoit Côté[1,2,3,4*], Marius Eichler[5], Andrés Yagüe[1], Nicole Vassh[6,3], Matthew R. Mumpower[7,8,3], Blanka Világos[1], Benjámin Soós[1], Almudena Arcones[5,9], Trevor M. Sprouse[6,7], Rebecca Surman[6,3], Marco Pignatari[10,1,3,4], Benjamin Wehmeyer[1,11], Thomas Rauscher[11,12], Maria Lugaro[1,13]

[1]Konkoly Observatory, Research Centre for Astronomy and Earth Sciences, Konkoly Thege Miklos ut 15-17, H-1121 Budapest, Hungary

[2]National Superconducting Cyclotron Laboratory, Michigan State University, East Lansing, MI 48824, USA

[3]Joint Institute for Nuclear Astrophysics - Center for the Evolution of the Elements, USA

[4]NuGrid Collaboration, https://nugrid.github.io

[5]Institut für Kernphysik, Technische Universität Darmstadt, Schlossgartenstrasse 2, D-64289 Darmstadt, Germany

[6]Department of Physics, University of Notre Dame, Notre Dame, Indiana 46556, USA

[7]Theoretical Division, Los Alamos National Laboratory, Los Alamos, NM, 87545, USA

[8]Center for Theoretical Astrophysics, Los Alamos National Laboratory, Los Alamos, NM, 87545, USA

[9]GSI Helmholtzzentrum fr Schwerionenforschung GmbH, Planckstr. 1, Darmstadt D-64291, Germany

[10]E.A. Milne Centre for Astrophysics, University of Hull, Hull, HU6 7RX

[11]Centre for Astrophysics Research, University of Hertfordshire, College Lane, Hatfield AL10 9AB, United Kingdom

[12]Department of Physics, University of Basel, Klingelbergstrasse 82, 4056 Basel, Switzerland

[13]Monash Centre for Astrophysics, School of Physics and Astronomy, Monash University, VIC 3800, Australia

*To whom correspondence should be addressed; E-mail: benoit.cote@csfk.mta.hu.

Meteoritic analysis demonstrates that radioactive nuclei heavier than iron were present in the early Solar System [1]. Among them, ^{129}I and ^{247}Cm both have a rapid neutron-capture process (r process) origin [2,3] and decay on the same timescale ($\simeq$ 15.6 Myr). We show that the $^{129}\mathrm{I}/^{247}\mathrm{Cm}$ abundance ratio in the early Solar System (438 ± 184) is immune to galactic evolution uncertainties and represents the first direct observational constraint for the properties of the last r-process event that polluted the pre-solar nebula. We investigate the physical conditions of this event using nucleosynthesis calculations and demonstrate that moderately neutron-rich ejecta can produce the observed ratio. We conclude that a dominant contribution by exceedingly neutron-rich ejecta is highly disfavoured.

The rapid neutron-capture process (r process) is believed to be the source in the Galaxy of half of the naturally occurring isotopes heavier than iron. Examples of elements dominated by r-process contributions are iodine, europium, gold, platinum, and the actinides. However, the physical conditions in which the r-process elements have been synthesized in the Universe, as well as which astrophysical sites can host the r process, are still a matter of debate.

The gravitational wave detection GW170817 by LIGO/Virgo [4] and the connection between its light curve and the presence of lanthanide elements [5, 6], such as europium, showed that neutron star mergers can synthesize at least some r-process elements. However, it only provided limited information on the nucleosynthesis, as no signature of a specific element or isotope has been directly probed, except for strontium [7]. To recover detailed isotopic information for the r-process nucleosynthesis, we can instead exploit the composition of our Solar System. Thanks to the analysis of primitive meteorites, our Solar System is currently the only system in the Universe for which we can derive abundances for all stable isotopes [8]. The measured solar composition can therefore be used to address aspects of the production of r-process

elements that cannot be probed by any other astronomical object. Abundances derived from the surface of other stars typically provide elemental abundances only [9].

Disentangling the origin of the solar stable isotopic composition, however, requires the use of Galactic chemical evolution simulations that follow the contribution of all different nucleosynthetic events (supernovae, compact binary mergers, etc.) from all stellar generations that lived and died prior to the formation of the Sun. The uncertainties involved in the modeling of such evolution can be reduced by considering radioactive isotopes with half-lives of the order of millions of years (Myr). Meteoritic analysis reveals the presence of such isotopes at the time of the formation of the first solids (the calcium-aluminium-rich inclusions, CAIs) in the early Solar System[1] [1]. Because they decay relatively fast relative to Galactic timescales, these radioactive isotopes carry the signature of a smaller number of nucleosynthesis events compared to stable isotopes, probing events closer in time to the formation of the Sun. In this work, we focus on the abundances in the early Solar System of two "short-lived" (half-lives of 15.6 Myr) radioactive isotopes: ^{129}I, which is located in the second r-process peak of the Solar System r-process distribution, and the much heavier actinide isotope, ^{247}Cm. The relative abundances of these isotopes, inferred from high-precision meteoritic analysis, are shown in Table 1.

Predicting isotopic ratios with Galactic chemical evolution simulations and connecting them to actual nucleosynthetic events is subject to many uncertainties. For instance, the abundance ratio ^{129}I / ^{127}I has a stable isotope in the denominator, which traces the full Galactic chemical evolution history prior to the formation of the Solar System. This ratio is therefore affected by uncertainties such as the star formation history, the amount of interstellar gas within the Milky Way, and the amount of ^{127}I removed from the interstellar gas by large-scale galactic outflows [13]. The ^{247}Cm / ^{235}U ratio is less affected by galactic evolution uncertainties because the longest-lived isotope of the ratio, ^{235}U, only has a half-life of 704 Myr, which is short

[1]Those radioactive abundances, today all extinct, are traced by the excess of the abundances of the daughter stable isotopes that the radioactive isotopes decay into.

Short-lived radionuclide	Half-life (Myr)	Reference nucleus	Half-life (Myr)	Early Solar System ratio	Refs.
^{129}I	15.7 ± 0.8	^{127}I	stable	$(1.28 \pm 0.03) \times 10^{-4}$	[10]
^{247}Cm	15.6 ± 1.0	^{235}U	704 ± 2	$(5.6 \pm 0.3) \times 10^{-5}$	[11, 12]
^{129}I	15.7 ± 0.8	^{247}Cm	15.6 ± 1.0	438 ± 184	See main text

Table 1. Radioactive nuclei produced by the r process that were present at the time of the formation of the Solar System for which we have high-precision data ($2\sigma < 6\%$) on their half-lives, their reference isotopes, and their early Solar System ratio. All errors are given at 2σ. The 45% error on the ^{129}I / ^{247}Cm is dominated by the 40% (2σ) uncertainty on the Solar System elemental abundance of I. ^{244}Pu (80 Myr) is not included here as its early Solar System abundance suffers from systematic uncertainties by roughly a factor of 2 [1].

relative to Galactic timescales. However, recovering the original r-process nucleosynthetic ratio for ^{247}Cm / ^{235}U is still affected by the uncertain time interval that elapses between the time when these isotopes are created in their stellar source and the time when they condense into the first solids in the early Solar System. During this period of time, which is of the order of $100 - 200$ Myr for r-process isotopes [13–15] (see Supplementary Text), ^{247}Cm and ^{235}U decay exponentially. Because their half-lives differ by a factor of 50, the ^{247}Cm / ^{235}U abundance ratio will strongly diverge from its original value before being locked into the solids.

An additional complication arises from the fact that the enrichment of the interstellar gas from which the Solar System formed was not continuous, but stochastic and sometimes unpredictable [15–18]. It is difficult to derive with confidence the exact number of enrichment events encoded in the isotopic ratios derived from meteorites. And because the radioactive abundances from each of those events have decayed for an unknown amount of time, the relative contribution of each event to the radioactive composition of the early Solar System is even more challenging to quantify. Probing the astrophysical conditions and the nature of the r-process events that polluted the pre-solar nebula is therefore not straightforward when using the isotopic ratios mentioned above.

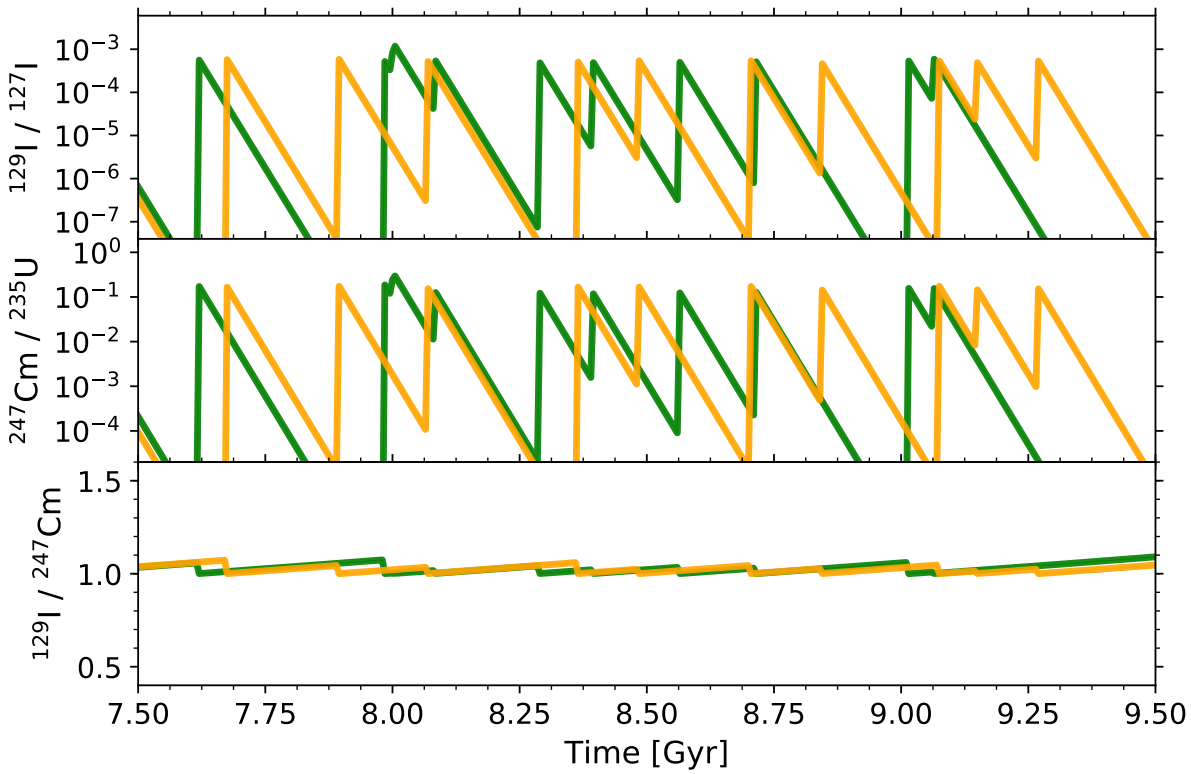

Fig. 1. Evolution of the abundance ratios ^{129}I/^{127}I, ^{247}Cm/^{235}U, and ^{129}I/^{247}Cm in a given parcel of gas inside our Galaxy around the time the Sun formed. Each peak is a new r-process event depositing radioactive material. The green and orange lines show two arbitrary Monte Carlo realisations for the temporal distribution of those events [19]. Each event is assumed to eject a flat isotope distribution with production ratios of 1. In a Galactic context, ^{129}I/^{127}I and ^{247}Cm/^{235}U vary by orders of magnitude, while ^{129}I/^{247}Cm varies by less than 10% and remains close to the production ratio.

However, using the ^{129}I/^{247}Cm abundance ratio bypasses all the uncertainties presented above. This is because ^{129}I and ^{247}Cm have the same half-life, within the uncertainties, so that their ratio is not strongly affected by the passage of time (see Fig. 1). This means that the ratio does not substantially change between the enrichment events and the formation of solids. Furthermore, because these isotopes are both short-lived compared to Galactic timescales, their ratio most likely carries the signature of only one r-process event (see Supplemental Text). We obtain the ^{129}I/^{247}Cm ratio in the early Solar System (see Table 1) using the reported ^{129}I/^{127}I

and ^{247}Cm / ^{235}U ratios, together with the ^{127}I / ^{235}U ratio of 189 [8]. This ^{129}I / ^{247}Cm ratio of 438 is a direct window into the nucleosynthesis of the last r-process event that polluted the pre-solar nebula, and provides new and unique insights for the physical conditions in which the r process can occur in nature.

We consider the ^{129}I / ^{247}Cm abundance ratios predicted by theoretical nucleosynthesis calculations based on the physical conditions extracted from hydrodynamic simulations of a variety of potential r-process sites: dynamical and disk ejecta from neutron star $-$ neutron star (NSNS) mergers and neutron star $-$ black hole (NSBH) mergers, and magneto-rotational-driven supernovae (MR SNe). We considered three NSNS and NSBH merger dynamical ejecta simulations from two research groups [20–23] and three NSNS merger disk simulations with varying initial conditions [24, 25]. For MR SNe, we used the simulation of Ref. [26]. We refer to Table S1 for more details on those seven simulations. Since r-process nucleosynthesis predictions bear large uncertainties from unknown nuclear physics properties [27–29], we repeated our calculations using three different sets of nuclear reaction rates and three different models for the distribution of fission fragments (see Methods). This generated a total of nine nucleosynthetic model predictions that are consistently applied to each of the seven hydrodynamic simulations.

In Fig. 2, we compare our predicted ^{129}I / ^{247}Cm ratios against the meteoritic ratio. For each hydrodynamic simulation, the plotted range of nucleosynthesis predictions encompasses the values obtained using the different nuclear physics input mentioned above. The meteoritic ratio shown in this figure represents the nucleosynthesis product of the last r-process event. The error bars on the meteoritic ratio (red horizontal bands) include both the uncertainty in the derivation of the early Solar System ratio (see Table 1) and the uncertainty in the half-lives of ^{129}I and ^{247}Cm. We include the latter to account for the slight ratio variation that could have occurred during the time elapsed between the last r-process event and the condensation of the first solids in the early Solar System (see Methods).

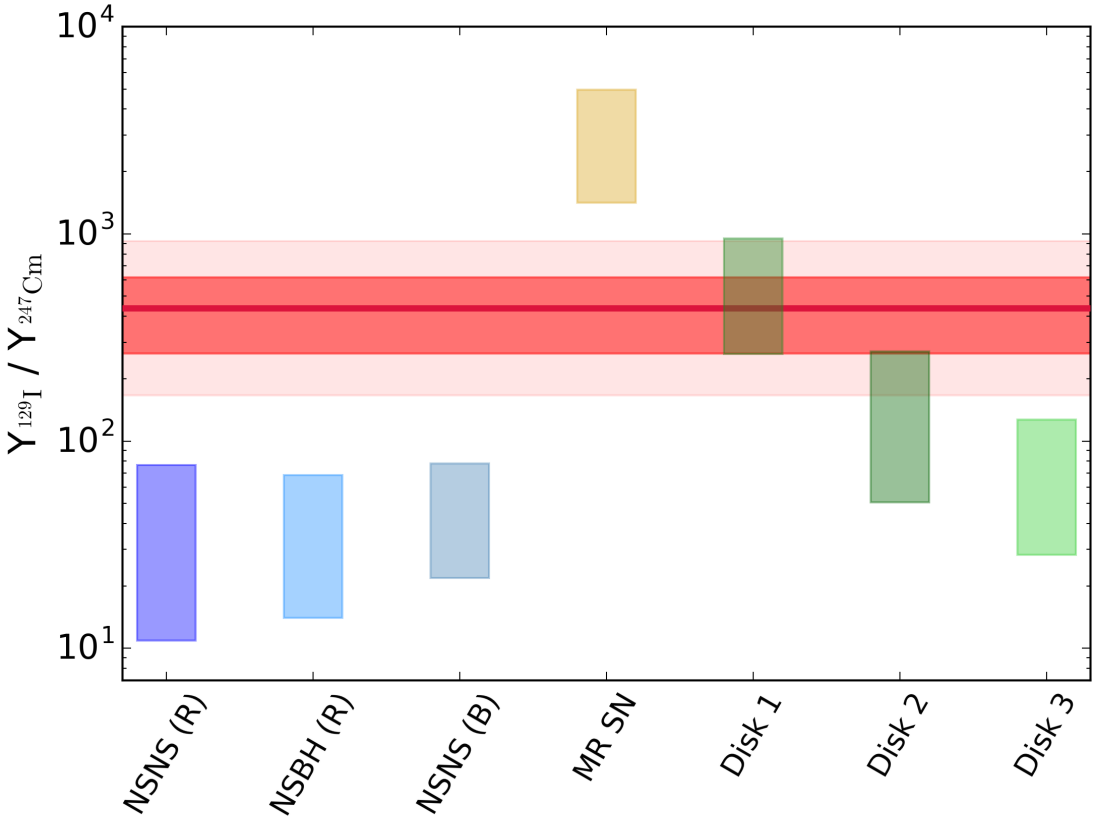

Fig. 2. ^{129}I / ^{247}Cm abundance ratios predicted by our theoretical r-process models (see Methods section). The red horizontal line and horizontal bands show the meteoritic ratio along with its 1σ and 2σ uncertainty (see Methods section).

Since ^{129}I belongs to the second r-process peak while ^{247}Cm belongs to the actinides, their relative abundances strongly depend on the physical conditions in which the nucleosynthesis occurs. In fact, the range of predicted ratios covered by all scenarios shown in Fig. 2 spans more than two orders of magnitude. In the case of the NSNS and NSBH merger simulations considered here, dynamical ejecta are dominated by very neutron-rich conditions and the actinides (such as ^{247}Cm) are produced more significantly relatively to the lighter nuclei (^{129}I in this case), as compared to the other r-process scenarios (see also Fig. S2). As a result, their ^{129}I / ^{247}Cm ratios are all smaller than 100, which is below the 2σ uncertainty band derived for the meteoritic

ratio. Similarly, Ref. [30] showed that dynamical ejecta overproduce the Th/Eu elemental ratio derived from the surface of actinide-boost stars, which suggests that very neutron-rich conditions cannot entirely be responsible for the enrichment of these stars. Although current merger simulations tend to predict the presence of very neutron-rich material, these simulations still an active area of research, such that the dominance of very neutron-rich conditions in dynamical ejecta remains debatable.

For the MR SN ejecta of Ref. [26], the abundance ratio is always larger than 1000 because most of the ejecta are not sufficiently neutron-rich to produce the actinides in significant amounts. We expect that other and next-generation MR SN simulations may generate different $^{129}\mathrm{I}/^{247}\mathrm{Cm}$ ratios. However, recent models with improved neutrino transport lead to more pessimistic predictions for the production of actinides [31]. For the three accretion-disk ejecta considered in Fig. 2, Disk 1 is remarkably consistent with the meteoritic value, Disk 2 just overlaps with the 2σ uncertainty band, while Disk 3 is below the 2σ uncertainty band and therefore not compatible.

To reinforce the suggested behavior of Fig. 2, we performed further nucleosynthesis calculations on the dynamical ejecta of Refs. [20–22] using a different nucleosynthesis code along with a wider input variety of 14 nuclear physics models (see Methods). As shown in Tables S2 and S3, the vast majority of those predictions have $^{129}\mathrm{I}/^{247}\mathrm{Cm}$ ratios below 100, which is consistent with the results presented in Fig. 2, except for a small number of cases, for which dynamical ejecta could reach the meteoritic ratio. This highlights the need for reducing nuclear physics uncertainties. Overall, our additional calculations confirm that the scenario where the pre-solar nebula was predominantly enriched by very neutron-rich ejecta is strongly disfavoured. This result applies to the last r-process event that polluted the pre-solar nebula with radioactive isotopes, not to the collective contribution of all previous events that built up the stable r-process solar composition.

So far we have considered every r-process site as independent. Another complication is that the portion of the ejecta which was introduced into the pre-solar nebula may not represent the full ejecta from the r-process source(s). If we assume this portion of ejecta to be representative of the event(s), a possible way to generate a ratio similar to the meteoritic value could be that the enrichment was a mixture of scenarios. However, we find that a mixture of dynamical and MR SN ejecta is very unlikely, with an occurrence probability of less than 10% (see Supplementary Text). We should also consider that the full ejecta of a compact binary merger is composed of both dynamical and disk ejecta [5, 32]. Even if Disk 1 is already consistent with the meteoritic value, the uncertainties in the measured and modeled values allow us to build a mixture of dynamical and disk ejecta within the observed error bars. Although such an investigation is affected by nuclear physics uncertainties, selecting as a test case the set of nuclear physics input that produces the highest ratio for both Disk 1 and the dynamical ejecta of Ref. [23] (dyn. NSNS (B)), we found that the maximum allowed contribution of dynamical ejecta to generate a ratio at the 2σ lower limit of the meteoritic value is 46%, in mass fraction.

Despite the nuclear astrophysics uncertainties involved when interpreting the site origin of meteoritic abundance ratios, the ^{129}I/^{247}Cm abundance ratio is immune to galactic evolution uncertainties and provides for the first time a direct view into the nucleosynthesis of an r-process event that occurred in our Galaxy. This is the only meteoritic ratio that can probe with such high confidence the physical conditions of the last r-process event that polluted the pre-solar nebula. Our results currently favour moderately neutron-rich ejecta over very neutron-rich ejecta, but hydrodynamic simulations and nuclear physics are continuously improving. We therefore expect the ^{129}I/^{247}Cm abundance ratio to become an important diagnostic tool for next-generation r-process nucleosynthesis calculations.

References

1. M. Lugaro, U. Ott, Á. Kereszturi, *Progress in Particle and Nuclear Physics* **102**, 1 (2018).

2. J. J. Cowan, *et al.*, *arXiv e-prints* (2019).

3. C. J. Horowitz, *et al.*, *Journal of Physics G Nuclear Physics* **46**, 083001 (2019).

4. B. P. Abbott, *et al.*, *Physical Review Letters* **119**, 161101 (2017).

5. P. S. Cowperthwaite, *et al.*, *ApJ* **848**, L17 (2017).

6. M. R. Drout, *et al.*, *Science* **358**, 1570 (2017).

7. D. Watson, *et al.*, *arXiv e-prints* p. arXiv:1910.10510 (2019).

8. K. Lodders, *Astrophysics and Space Science Proceedings* **16**, 379 (2010).

9. C. M. Sakari, *et al.*, *ApJ* **868**, 110 (2018).

10. J. D. Gilmour, O. V. Pravdivtseva, A. Busfield, C. M. Hohenberg, *Meteoritics and Planetary Science* **41**, 19 (2006).

11. F. L. H. Tissot, N. Dauphas, L. Grossman, *Science Advances* **2**, e1501400 (2016).

12. H. Tang, M.-C. Liu, K. D. McKeegan, F. L. H. Tissot, N. Dauphas, *Geochim. Cosmochim. Acta* **207**, 1 (2017).

13. B. Côté, *et al.*, *ApJ* **878**, 156 (2019).

14. M. Lugaro, *et al.*, *Science* **345**, 650 (2014).

15. T. Tsujimoto, T. Yokoyama, K. Bekki, *ApJ* **835**, L3 (2017).

16. K. Hotokezaka, T. Piran, M. Paul, *Nature Physics* **11**, 1042 (2015).

17. Y. Fujimoto, M. R. Krumholz, S. Tachibana, *MNRAS* **480**, 4025 (2018).

18. I. Bartos, S. Marka, *Nature* **569**, 85 (2019).

19. B. Côté, A. Yagüe, B. Világos, M. Lugaro, *arXiv e-prints* p. arXiv:1911.01457 (2019).

20. O. Korobkin, S. Rosswog, A. Arcones, C. Winteler, *MNRAS* **426**, 1940 (2012).

21. T. Piran, E. Nakar, S. Rosswog, *MNRAS* **430**, 2121 (2013).

22. S. Rosswog, T. Piran, E. Nakar, *MNRAS* **430**, 2585 (2013).

23. L. Bovard, *et al.*, *Phys. Rev. D* **96**, 124005 (2017).

24. M.-R. Wu, R. Fernández, G. Martínez-Pinedo, B. D. Metzger, *MNRAS* **463**, 2323 (2016).

25. J. Lippuner, *et al.*, *MNRAS* **472**, 904 (2017).

26. C. Winteler, *et al.*, *ApJ* **750**, L22 (2012).

27. M. Eichler, *et al.*, *ApJ* **808**, 30 (2015).

28. M. R. Mumpower, R. Surman, G. C. McLaughlin, A. Aprahamian, *Progress in Particle and Nuclear Physics* **86**, 86 (2016).

29. N. Vassh, *et al.*, *Journal of Physics G Nuclear Physics* **46**, 065202 (2019).

30. E. M. Holmbeck, *et al.*, *ApJ* **881**, 5 (2019).

31. P. Mösta, *et al.*, *ApJ* **864**, 171 (2018).

32. B. D. Metzger, E. Berger, *ApJ* **746**, 48 (2012).

33. C. Freiburghaus, S. Rosswog, F. K. Thielemann, *ApJ* **525**, L121 (1999).

34. R. H. Cyburt, *et al.*, *ApJS* **189**, 240 (2010).

35. P. Möller, J. R. Nix, W. D. Myers, W. J. Swiatecki, *Atomic Data and Nuclear Data Tables* **59**, 185 (1995).

36. P. Möller, B. Pfeiffer, K.-L. Kratz, *Phys. Rev. C* **67**, 055802 (2003).

37. M. R. Mumpower, T. Kawano, P. Möller, *Phys. Rev. C* **94**, 064317 (2016).

38. T. Marketin, L. Huther, G. Martínez-Pinedo, *Phys. Rev. C* **93**, 025805 (2016).

39. J. Duflo, A. P. Zuker, *Phys. Rev. C* **52**, R23 (1995).

40. M. Eichler, W. Sayar, A. Arcones, T. Rauscher, *ApJ* **879**, 47 (2019).

41. J. Beun, G. C. McLaughlin, R. Surman, W. R. Hix, *Phys. Rev. C* **77**, 035804 (2008).

42. I. V. Panov, C. Freiburghaus, F.-K. Thielemann, *Nuclear Physics A* **688**, 587 (2001).

43. T. Kodama, K. Takahashi, *Nuclear Physics A* **239**, 489 (1975).

44. A. Kelic, M. Valentina Ricciardi, K.-H. Schmidt, *arXiv e-prints* (2009).

45. M. R. Mumpower, *et al.*, *ApJ* **869**, 14 (2018).

46. G. Audi, F. Kondev, M. Wang, W. Huang, S. Naimi, *Chin. Phys. C* **41**, 030001 (2017).

47. W. D. Myers, W. J. Swiatecki, *Phys. Rev. C* **60**, 014606 (1999).

48. A. Mamdouh, J. M. Pearson, M. Rayet, F. Tondeur, *Nucl. Phys. A* **679**, 337 (2001).

49. S. Goriely, *Tours Symposium on Nuclear Physics V*, M. Arnould, *et al.*, eds. (2004), vol. 704 of *American Institute of Physics Conference Series*, pp. 375–384.

50. P. Möller, A. J. Sierk, T. Ichikawa, A. Iwamoto, M. R. Mumpower, *Phys. Rev. C* **91**, 024310 (2015).

51. T. Kawano, P. Möller, W. B. Wilson, *Phys. Rev. C* **78**, 054601 (2008).

52. T. Kawano, R. Capote, S. Hilaire, P. Chau Huu-Tai, *Phys. Rev. C* **94**, 014612 (2016).

53. M. R. Mumpower, *et al.*, *Phys. Rev. C* **92**, 035807 (2015).

54. K.-H. Schmidt, B. Jurado, C. Amouroux, C. Schmitt, *Nucl. Data Sheets* **131**, 107 (2016).

55. P. Möller, M. R. Mumpower, T. Kawano, W. D. Myers, *At. Data Nucl. Data Tables* **125**, 1 (2019).

56. J. Abadie, *et al.*, *Classical and Quantum Gravity* **27**, 173001 (2010).

57. C. Kim, B. B. P. Perera, M. A. McLaughlin, *MNRAS* **448**, 928 (2015).

58. B. S. Meyer, D. D. Clayton, *Space Sci. Rev.* **92**, 133 (2000).

59. B. Côté, *et al.*, *ApJ* **836**, 230 (2017).

60. A. Wallner, *et al.*, *Nature Communications* **6**, 5956 (2015).

61. D. D. Clayton, *ApJ* **285**, 411 (1984).

62. G. R. Huss, B. S. Meyer, G. Srinivasan, J. N. Goswami, S. Sahijpal, *Geochim. Cosmochim. Acta* **73**, 4922 (2009).

63. B. G. Elmegreen, J. Scalo, *ARA&A* **42**, 211 (2004).

64. M. G. H. Krause, *et al.*, *A&A* **619**, A120 (2018).

65. A. Emerick, *et al.*, *ApJ* **869**, 94 (2018).

66. D. Rennehan, A. Babul, P. F. Hopkins, R. Davé, B. Moa, *MNRAS* **483**, 3810 (2019).

67. I. U. Roederer, *et al.*, *ApJ* **698**, 1963 (2009).

68. E. M. Holmbeck, *et al.*, *ApJ* **859**, L24 (2018).

Acknowledgments

We thank Mária Pető for discussion. This research is supported by the ERC Consolidator Grant (Hungary) funding scheme (Project RADIOSTAR, G.A. n. 724560), the Hungarian Academy of Sciences via the Lendület project LP2014-17, and the ChETEC COST Action (CA16117), supported by COST (European Cooperation in Science and Technology). BC, MM, and MP acknowledge support from the National Science Foundation (NSF, USA) under grant No. PHY-1430152 (JINA Center for the Evolution of the Elements). MM was supported by the US Department of Energy through the Los Alamos National Laboratory. Los Alamos National Laboratory is operated by Triad National Security, LLC, for the National Nuclear Security Administration of U.S. Department of Energy (Contract No. 89233218CNA000001). MM was also supported by the Laboratory Directed Research and Development program of Los Alamos National Laboratory under project number 20190021DR. ME and AA acknowledge support from European Research Council through ERC Starting Grant No. 677912 EUROPIUM and Deutsche Forschungsgemeinschaft through SFB 1245. The work of NV and RS was supported by the Fission In R-process Elements (FIRE) topical collaboration in nuclear theory, funded by the U.S. Department of Energy. The work of TS and RS was also supported by the U.S. Department of Energy SciDAC collaboration TEAMS (de-sc0018232). TS was additionally supported by the Los Alamos National Laboratory Center for Space and Earth Science, which is funded by its Laboratory Directed Research and Development program under project number 20180475DR. MP acknowledges support from STFC (through the University of Hull's Consol-

idated Grant ST/R000840/1), and access to VIPER, the University of Hull High Performance Computing Facility. This work has benefited from discussions at the 2019 Frontiers in Nuclear Astrophysics Conference supported by the JINA Center for the Evolution of the Elements, and at conferences supported by the ChETEC (Chemical Elements as Tracers of the Evolution of the Cosmos) COST Action (CA16117, European Cooperation in Science and Technology).

Supplementary Materials

Methods

Nuclear Physics Uncertainties

The r process proceeds via a synthesis of very neutron-rich isotopes that are currently inaccessible by experimental nuclear physics facilities. Calculations therefore must rely on theoretical data for the reaction and decay processes which determine the abundances of ^{129}I and ^{247}Cm. Since such theoretical data can vary greatly outside experimentally probed nuclei, this introduces uncertainties in the predicted ^{129}I / ^{247}Cm ratio.

In the case of ^{247}Cm production, we find that this depends mostly on the model strength of the N = 126 shell closure [2], which determines how r-process material proceeds into the actinide region, along with the β-decay treatment which determines the decay path of nuclei which eventually populate this species. Currently available theoretical fission treatments suggest fission to not greatly impact the production of ^{247}Cm since it lies in a region of the nuclear chart just below where fission typically begins to participate in the r process, however α-decay feeding from heavier species introduces a small sensitivity to how fission is treated at higher mass numbers. In contrast, the production of ^{129}I is influenced by the fission treatment via the fission fragment distributions of heavy, neutron-rich species which can deposit into the second r-process peak,

[2] N refers to the number of neutrons.

but is also dependent on the predicted structure of the N = 82 shell closure. All of these pieces of nuclear data governing how ^{129}I and ^{247}Cm are populated in the r process have yet to be determined experimentally.

Nucleosynthesis Models

The nucleosynthesis results presented in Fig. 2 have been obtained with the nuclear network code WINNET [26]. For each hydrodynamic simulation (see Table S1 for setup details), we post-processed all tracer particles that recorded the evolution of the physical conditions (density and temperature) as a function of time within different parts of the ejecta. Those temporal profiles are typically referred to as *trajectories* and represent the fundamental inputs for our nucleosynthesis calculations. During the post-processing, we included the additional heating caused by nuclear reactions, following the description of Ref. [33]. Wherever possible, we used experimental nuclear reaction rates, but most of the nuclear physics input necessary for r-process nucleosynthesis calculations is based on theoretical models that are still rather uncertain for nuclei far from stability.

To illustrate the impact of nuclear physics uncertainties, we repeated all of our calculations using nine combinations of nuclear physics input. For the first set, labeled FRDM, we used the default JINA Reaclib reaction rate library[3] [34] with reaction rates based on the Finite-Range Droplet Model (FRDM) [35]. For the second set, labeled FRDM(D3C*), we used JINA Reaclib but replaced the default theoretical β-decay rates of Refs. [36, 37] with those of Ref. [38]. For the third set, labeled DZ10, we used neutron-capture and charged-particle rates (and their reverse reactions) based on the Duflo-Zuker mass model with 10 parameters [39], together with the β-decay rates of Refs. [36, 37]. The complete setup for those sets is summarized in Table 1 of Ref. [40]. The possible fission of actinides in very neutron-rich conditions [20, 41] adds another layer of nuclear physics uncertainty to our predictions [29]. To test this, for each input set

[3] http://reaclib.jinaweb.org/; version from 10/20/2017

(FRDM, FRDM(D3C*), and DZ10), we ran our nucleosynthesis calculations with three different fission fragment distribution models: Panov et al. (2001) labeled as Panov [42], Kodama & Takahashi (1975) labeled as K & T [43], and the ABLA07 model [44].

Fig. S1 is a version of Fig. 2 where we explicitly show the ^{129}I / ^{247}Cm ratios predicted using the nine different nuclear physics model combinations described above. For each site (i.e., hydrodynamic simulation), the large, opaque symbols show the isotopic composition of the total ejected mass, while the smaller, transparent symbols represent trajectories for individual parts of the ejecta that build up the total ejecta. Although the total ejecta are the most relevant quantities to focus on for the purpose of this study (see Fig. 2), the different trajectories illustrate the wide range of physical conditions that can take place within a single r-process event.

Additional Calculations for Dynamical Ejecta

Since the nucleosynthesis calculations presented in Fig. 2, and outlined in more detail in Fig. S1, strongly suggest that very neutron-rich dynamical ejecta (dyn. NSNS (R) and dyn. NSBH (R)) produce ^{129}I / ^{247}Cm ratios below the meteoritic value, we performed additional, independent network calculations to investigate this conclusion. To do so, we used the nucleosynthesis network PRISM developed jointly at the University of Notre Dame and the Los Alamos National Laboratory [45]. We applied experimentally known decay rates from NUBASE2016 [46] where available. For theoretical nuclear data, we considered ten mass models (FRDM2012, FRDM1995, DZ33, Thomas-Fermi (TF), ETFSI, ETFSI-Q, HFB-17, HFB-21, SLY4, and UNEDF0) matched with the most appropriate available fission barrier set (TF barriers [47] are applied with TF masses, ETFSI barriers [48] with ETFSI masses, HFB barriers [49] with HFB masses, and FRLDM barriers [50] in all other cases). We used the statistical Hauser-Feshbach framework from Ref. [37, 51, 52] to produce neutron-capture, β-decay, neutron-induced fission and β-delayed fission rates which are consistent with the theoretical masses and fission barriers

as in Refs. [29, 53]. For the fission yields of heavy neutron-rich nuclei, we used GEF2016 [54]. As was done with WINNET calculations, for a selection of mass models, we considered β-decay rates derived from both the Möller QRPA [55] and D3C* [38] frameworks.

The PRISM results for the ^{129}I / ^{247}Cm ratio with the different theoretical data sets are given in Tables S2 and S3. When using Möller QRPA β-decay, the ranges given by the simulation trajectories are typically lower than the meteoritic ^{129}I / ^{247}Cm ratio, with ETFSI-Q predicting the highest possible value. The mass weighted average of all trajectories lies below the meteoritic ratio for all models. When using D3C* β-decay, however, the nuclear data combination of TF masses and fission barriers predicts ^{129}I / ^{247}Cm ratios that are consistent with the meteoritic value. Our calculations suggest that although very neutron-rich conditions in dynamical ejecta cannot be entirely ruled out as the last pre-solar r-process source, such conditions are strongly disfavoured by current mass models.

Error Bars of the Observed ^{129}I / ^{247}Cm Ratio

To compare meaningfully with our nucleosynthesis predictions, the ^{129}I / ^{247}Cm ratio derived from meteoritic analysis must reflect the nucleosynthesis production of the last r-process event. As described in the main text, because ^{129}I and ^{247}Cm have very similar mean lives, their ratio did not vary significantly between the time when the r-process event that produced them occurred and the formation of the first solids in the early Solar System. This time interval can be determined using the ^{129}I / ^{127}I and ^{247}Cm / ^{235}U ratios, and is currently estimated to be between 100 and 200 million years (Myr) (See Supplementary Text).

The mean lives of ^{129}I and ^{247}Cm have 2σ uncertainties of 5% and 6%, respectively, and their isotopic ratio decays with an equivalent mean life

$$\tau_{\rm eq} = \frac{\tau_1 \tau_2}{(\tau_2 - \tau_1)}, \tag{1}$$

where τ_1 and τ_2 represents the mean life of ^{129}I and ^{247}Cm, respectively. We derived the prob-

ability distribution function of $\tau_{\rm eq}$ by running Monte Carlo calculations where we randomly sampled the mean lives of ^{129}I and ^{247}Cm individually assuming a normal distribution based on their 2σ uncertainty (see Table 1). We found that $\tau_{\rm eq}$ ranges from $\sim$ 100 Myr to several billion years. The relatively short timescales covered by the tail of the distribution implies the possibility that the ejected ^{129}I/^{247}Cm ratio could have somewhat deviated from its original value before being locked into solids.

To account for this possible variation, we decayed the Solar System value backward in time for 200 Myr using a Monte Carlo approach. In each run, we randomly sampled the equivalent mean life from the probability distribution of $\tau_{\rm eq}$, as well as the early Solar System value from a normal distribution based on the 2σ uncertainty presented in Table 1. After running this calculation 10 million times, we found values for the ^{129}I/^{247}Cm ratio between 300 and 700 at 1σ, and between 190 and 1100 at 2σ. These confidence intervals are shown in Figs. 2 and S1 and represent the uncertainty in the observed ^{129}I/^{247}Cm ratio, as it was just after the last r-process event that occurred prior the formation of the Solar System. Those are conservative error bars because our calculations suggest that the last r-process event occurred less than 200 Myr before the condensation of the first solids in the early Solar System (see Supplementary Text and Fig. S3).

Supplementary Text

Deriving Physical Conditions from the ^{129}I/^{247}Cm Ratio

As shown in Fig. S1, the isotopic ratio of the dynamical ejecta of Ref. [23] (dyn. NSNS (B)) is lower than the meteoritic value by roughly an order of magnitude. However, this model contains a significant number of individual trajectories (i.e., sets of physical conditions, see Methods) that cover a wide range of ratios, both lower and higher than the meteoritic value. Considering all those trajectories as a collection of possible physical conditions from which we

can sample, we searched for a combination of trajectories that would lead to the early Solar System value of 438 ± 92 (within 1σ uncertainty), as reported in Table 1.

To do so, we employed an iterative random sampling procedure (see also Ref. [30]). In each iteration, we randomly selected ten trajectories, summed the abundances of ^{129}I and ^{247}Cm, and calculated the integrated ^{129}I/^{247}Cm abundance ratio. If the ratio was in the allowed range of 438 ± 92, the ten trajectories were added to the sampled ejecta, and this process was repeated until the integrated ^{129}I/^{247}Cm ratio of the sampled ejecta did not change by more than a factor of 10^{-6} when ten new trajectories were added. This sampled ejecta therefore represents a subset of trajectories that, once combined together, fits the early Solar System ratio.

In Fig. S2, we show the distribution of electron fractions Y_e of the fitted ejecta. This quantity probes the amount of available neutrons, and is defined as follows,

$$Y_e = \frac{n_p}{n_n + n_p}, \tag{2}$$

where $n_{p/n}$ is the particle density of protons and neutrons, respectively. The lower Y_e is, the more neutron-rich are the conditions. As shown in Fig. S2, the Y_e distribution of the fitted ejecta is less neutron-rich than the original dynamical ejecta. In fact, the bulk of the fitted Y_e distribution is in between 0.2 and 0.3, with a very small contribution on the very neutron-rich side ($Y_e < 0.15$), which is the opposite of the original ejecta from which we sampled. We note that these fitted ejecta are not associated with any r-process site in particular, it only represents an example of what is needed to reproduce the ^{129}I/^{247}Cm ratio in the early Solar System. Nevertheless, and interestingly, the Y_e distribution of the fitted ejecta is comparable to the distribution of one of the disk ejecta of Refs. [24,25] (Disk 1), which successfully reproduces the early Solar System ^{129}I/^{247}Cm ratio (see Figs. 2 and S1). Using the different nuclear physics input labeled in Fig. S1 leads to similar conclusions.

Rarity of *r*-Process Events Nearby the Solar Neighborhood

An important ingredient in modeling the amount of r-process isotopes that was introduced into the pre-solar nebula, and in determining whether the $^{129}\mathrm{I}/^{247}\mathrm{Cm}$ ratio probes only one event, is the frequency of r-process events occurring in the solar neighborhood. For compact binary mergers (CBMs), even if there are some constraints for their cosmic and Galactic rates [4,56,57], it is still challenging to derive the frequency at which a given parcel of gas is expected to be enriched by those mergers. Back-of-the-envelope calculations suggest that regular core-collapse supernovae (CCSNe) could pollute a parcel of gas of the Milky Way every $5-10$ Myr, when considering a "snowplough" scenario [58]. Because CBMs are more rare than regular CCSNe by a factor of $\sim 100-1000$ [59], within the same scenario we expect the occurrence frequency of CBMs within a parcel of gas to be at least of the order of 500 Myr [1]. For rare classes of CCSNe capable of producing heavy r-process elements up to Cm, if they exist in nature, their frequency is even more uncertain.

Ref. [16] investigated the evolution of ^{244}Pu from the formation time of the Solar System until today, using a diffusive mixing prescription to spread radioactive isotopes throughout the interstellar medium. Their best model to explain the variation of ^{244}Pu observed across this time window, which is probed by meteoritic analysis and deep ocean crust measurements [60], involves rare r-process events that would occur every $\sim$500 Myr, on average, nearby the Sun. This low frequency was also derived by Ref. [15], while Ref. [18] obtained a somewhat lower value of $\sim$100 Myr when assuming a site four times more frequent.

Time Since the Last *r*-Process Event

Calculating the time elapsed between the last r-process event and the condensation of the first solids in the early Solar System, Δt_{LE}, allows us to decay backward the early Solar System $^{129}\mathrm{I}/^{247}\mathrm{Cm}$ ratio and recover the nucleosynthesis production of the last event (see Methods). For the r process, this can be done by predicting the isotopic ratios $^{129}\mathrm{I}/^{127}\mathrm{I}$ and $^{247}\mathrm{Cm}/^{235}\mathrm{U}$

in the parcel of gas from which the Sun formed, just after that last enrichment event, and decay them until they reach the early Solar System composition, which sets $\Delta t_{\rm LE}$ [1, 14]. Calculating $\Delta t_{\rm LE}$ also provides a consistency check for the nucleosynthesis models presented in Figs. 2 and S1. Not only a given model should be able to reproduce the ^{129}I/^{247}Cm ratio, the $\Delta t_{\rm LE}$ derived independently from ^{129}I/^{127}I and ^{247}Cm/^{235}U should also be the same, if ^{129}I and ^{247}Cm are co-produced by the same event.

Given the rarity of r-process events in the solar neighbourhood (see above), we start by considering that ^{129}I and ^{247}Cm in the early Solar System mostly came from one r-process event only (we quantitatively consider the likelihood of this assumption in the next section). In this case, their abundance ratio in the parcel of gas that constituted the pre-solar matter at time $T_{\rm gal}$ when the event occurred (where time zero is the birth of the Galaxy) is simply proportional to the respective nucleosynthesis yield, $Y_{^{129}\rm I}$ and $Y_{^{247}\rm Cm}$, of the event. The abundance of the stable ^{127}I, instead, reflects the contribution of all the previous r-process events that enriched the parcel of gas. Assuming an average time interval $\langle\delta\rangle$ between r-process events, the total number of ^{127}I isotopes within that parcel of gas is proportional to $Y_{^{127}\rm I}\left(\frac{T_{\rm gal}}{\langle\delta\rangle}\right)$. The iodine isotopic ratio can be written as [1, 14]

$$\frac{^{129}\rm I}{^{127}\rm I} = K_{\rm I}\left(\frac{Y_{^{129}\rm I}}{Y_{^{127}\rm I}}\right)\left(\frac{\langle\delta\rangle}{T_{\rm gal}}\right), \tag{3}$$

where $K_{\rm I}$ is a correction factor extracted from galactic chemical evolution models to account for the temporal evolution of the star formation rate in our Galaxy and the amount of stable isotopes locked inside stellar remnants [61, 62], as well as for the amount of stable isotopes ejected outside the Galaxy by galactic outflows [13]. The abundance of ^{235}U at $T_{\rm gal}$, because of its relatively long half-life, includes the contribution of several r-process events and is proportional to $Y_{^{235}\rm U}\left(\frac{1}{1-e^{-\langle\delta\rangle/\tau_{^{235}\rm U}}}\right)$, which leads to an isotopic ratio of

$$\frac{^{247}\rm U}{^{235}\rm U} = K_{\rm U}\left(\frac{Y_{^{247}\rm Cm}}{Y_{^{235}\rm U}}\right)\left(1-e^{-\langle\delta\rangle/\tau_{^{235}\rm U}}\right), \tag{4}$$

where $K_{\rm U}$ is equivalent to $K_{\rm I}$ but taking into account that ^{235}U is radioactive.

Fig. S3 shows our predictions for $\Delta t_{\rm LE}$ as a function of the recurrence time $\langle\delta\rangle$ between r-process events, using the correction factors $K_{\rm I}$ and $K_{\rm U}$ from the "best" galactic chemical evolution model of Ref. [13], and using the yields of three selected nucleosynthesis models presented in Fig. S1. The error bars represent the uncertainty band generated by the 2σ uncertainties in the half-life of ^{129}I and ^{247}Cm. Within a plausible range of $\langle\delta\rangle$ (see the previous section), the time between the condensation of solids in the early Solar System and the last r-process event ranges between 100 and 200 Myr. This range is consistent with previous estimates [13–15, 18].

For the dynamical ejecta of Ref. [23] (Dyn. NSNS (B)) and the disk ejecta of Refs. [24, 25] (Disk 1), the times derived from ^{129}I / ^{127}I and ^{247}Cm / ^{235}U are consistent with each other within the uncertainties, while it is not the case for the MR SN model of [26]. Using the different nuclear physics input shown in Fig. S1 does not alter those conclusions. This means the physical conditions met in Disk 1 can synthesize ^{129}I and ^{247}Cm in such a way that both isotopes trace back the same r-process event, in addition of being consistent with the ^{129}I / ^{247}Cm meteoritic ratio.

The experiment described above assumed that all r-process events generate the same nucleosynthesis product every time. But uncertainties in the nuclear physics and in the physical conditions of r-process calculations are currently too large (see, e.g., Disks 1, 2, and 3 in Figs. 2 and S1) to reliably include yield variations in our experiment. Once those uncertainties will be reduced, the calculation should be repeated to strengthen our conclusions. Finally, we note that our calculations do not consider explicitly any transport of material in the interstellar medium, but simply assume that all the isotopes are diluted by the same factor. Because such mixing processes are complex [63–66] and cannot properly be captured with non-hydrodynamic ap-

proaches, the timescales estimated above should be taken as first approximations.

Probability of Probing One *r*-Process Event

Metal-poor stars exhibit different levels of actinide enrichment relative to rare-Earth peak elements, as shown by their elemental ratio between thorium and europium [67, 68]. This indirectly suggests that actinide isotopes such as ^{247}Cm are not always synthesized in the same amount from one r-process event to another. Verifying quantitatively that the early Solar System ^{129}I/^{247}Cm ratio most likely encodes the signature of one event is therefore crucial for connecting this ratio to r-process nucleosynthesis calculations.

Ref. [19] investigated the stochastic evolution of radioactive isotopes in a given parcel of gas within the interstellar medium as a function of their mean life τ and the average time interval $\langle\delta\rangle$ between two consecutive enrichment events. They found that the probability of probing one event with a radioactive isotope varies from 0 to 100% when the timescale ratio $\tau/\langle\delta\rangle$ varies from 1 to 0.01. Because the mean life of ^{129}I and ^{247}Cm is 22.5 Myr, and because $\langle\delta\rangle$ for r-process events is probably between 100 and 500 Myr (see first part of Supplementary text), the $\tau/\langle\delta\rangle$ ratio is roughly between 0.05 and 0.2. According to Fig. 10 in Ref. [19], this range implies that for more than 90% of the time, 90% of the abundances of ^{129}I and ^{247}Cm in the interstellar medium were produced by only one event.

Ref. [18] also found that a single r-process event could account for 50 to 100% of all ^{247}Cm present in the early Solar System, using an approach similar to Ref. [16]. In addition, Ref. [15] suggested that this last r-process event could have contributed to about 80% the amount of ^{244}Pu present in the early Solar System, leaving a 20% contribution from other previous events. Since ^{244}Pu has a half-life five times longer than ^{129}I and ^{247}Cm, we expect that their models would predict the latter isotopes to be even more dominated by the last r-process event.

Possible Contribution by Two *r*-Process Events

To support the conclusions that ^{129}I / ^{247}Cm only probes one event, and to better understand the implications of probing multiple events, we designed a Monte Carlo experiment to calculate the possible contributions from the two last r-process events that preceded the formation of the Solar System, using a specific subset of the nucleosynthesis calculations presented in Fig. S1. For these tests, we used the dynamical ejecta of Ref. [23] (dyn. NSNS B), the MR-SN of Ref. [26], and the disk of Refs. [24, 25] (Disk 1), as these three models predict very different ^{129}I / ^{247}Cm ratios from one another (see Fig. S1). This allows us to quantify the chance that a mixture of two events matches the observed ratio, even if the single events do not. For all these models, we considered the ABLA07 fission fragment distribution model and the DZ10 mass model to make sure that one of our three models (Disk 1) precisely reproduces the meteoritic ratio. This allows us to quantify the chance of mixing a single non-matching event with a matching event, and remaining within the uncertainties of the observed ratio. We assumed that all events are independent and can occur at different times, even if disk and dynamical ejecta are ejected together in the case of compact binary mergers.

We start our calculations by randomly sampling two r-process events and separating them by a time delay δ. This delay is randomly sampled from the probability distribution functions calculated in Ref [19], which depend on the nature and average frequency of the enrichment source. We decay the ejecta of the first event for a time δ using an equivalent half-life $\tau_{\rm eq}$ drawn randomly from the distribution derived in the Methods section, based on the half-life uncertainties of ^{129}I and ^{247}Cm. Then, we mix the decayed ejecta of the first event with the ejecta of the second event (i.e., the last event before the formation of the Solar System). We then compare the mixture against the meteoritic ratio, which was already decayed backward in time to the last r-process event (see Methods). To decide whether the scenario is a successful realisation, we account for the probability distribution function of the meteoritic value, using a

Monte Carlo approach. This means the scenario has more chance to be picked if its ^{129}I / ^{247}Cm abundance ratio is close to the center of the meteoritic distribution, while it has less chance to be picked is its ratio falls on the tail of the meteoritic distribution (e.g., on the edge of the 2σ uncertainty band). We repeated this process many times to derive the probability of each successful scenario.

The results are summarized in Table S4. *All* refers to all the successful scenarios, while *Two disks*, *One disk*, and *No disk* refer to the number of disk event(s) among the two r-process events. Two percent estimates are reported in each cell of the table: the left-hand values were calculated by minimizing the chance of pollution by two events using an average frequency of 1 event per 500 Myr and a meteoritic ratio decayed backward for 100 Myr, as opposed to 200 Myr as shown in Figs. 2 and S1. The right-hand values were calculated by maximizing the chance of pollution by two events using a higher frequency of 1 event per 100 Myr and a meteoritic ratio decayed backward for 200 Myr. A longer decay time implies a larger 2σ uncertainty band for the meteoritic ratio, allowing more scenarios to be successful, and a higher event frequency enhances the chance of generating two events close-by in time.

Two main conclusions can be drawn from our experiment. First, there is less than 6% chance that two events other than a disk (*No disk* scenario) combine their ejecta to generate the observed value. Second, if the ejecta of one disk is mixed with another type of ejecta (*One disk* scenario), the probability for the disk to contribute to more than 99% the amount of ^{129}I and ^{247}Cm in the early Solar System is between $\sim$51 and 95%. And those probabilities increase to $\sim$84 and 98% when that contribution is lowered from 99 to 90%. The overall probability of probing two events with production ratios significantly different from the meteoritic value is highly disfavoured.

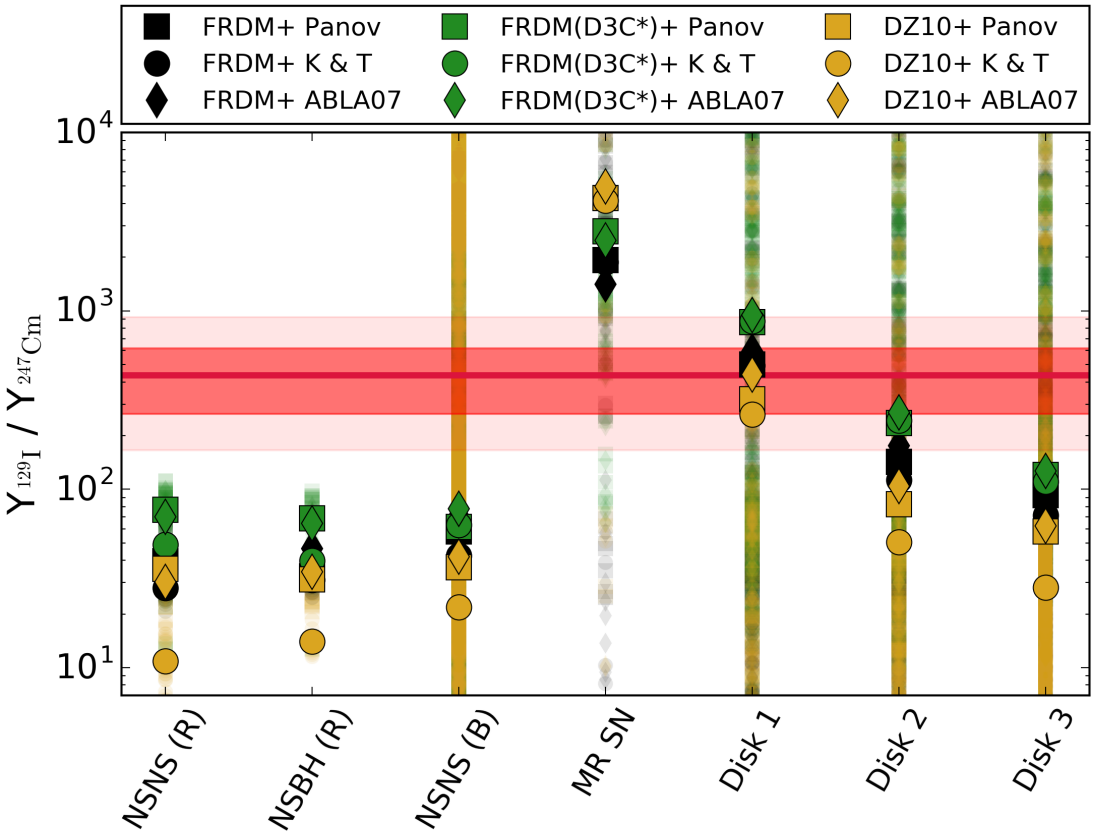

Fig. S1. ^{129}I / ^{247}Cm abundance ratios predicted by our theoretical r-process models. This figure is a more detailed version of Fig. 2, where the ratios from the individual trajectories are shown as small, transparent symbols, while the integrated ejecta are represented by the larger, opaque symbols. Different shaped symbols denote different fission fragment distribution models, while different colors denote different sets of nuclear reaction rates. We refer to the Methods section for more information. The meteoritic ratio along with the error bars are the same as in Fig. 2.

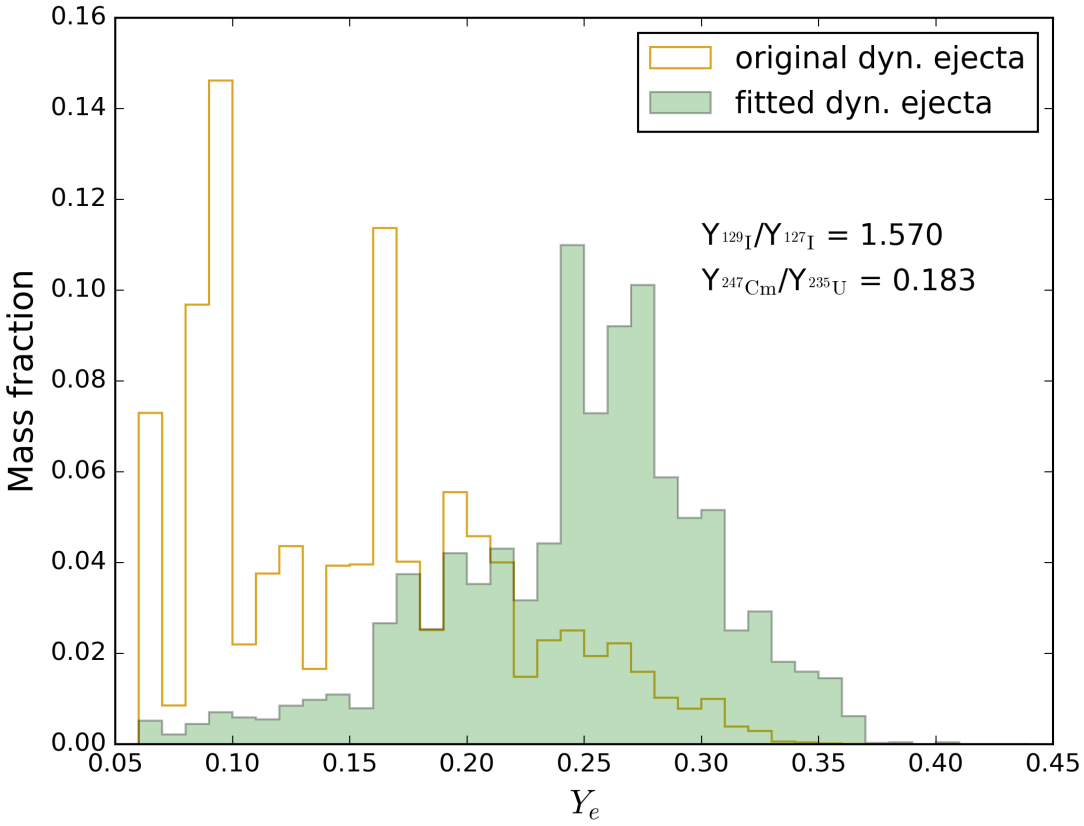

Fig. S2. Distribution of the electron fraction (Y_e) within the fitted r-process ejecta that successfully reproduced the early Solar System meteoritic $^{129}\mathrm{I}/^{247}\mathrm{Cm}$ ratio of 438 ± 92 (green histogram). This ejecta corresponds to the sum of a subset of the trajectories available with the dynamical ejecta of Ref. [23] (dyn. NSNS (B)), for which its original Y_e distribution, consisting of all trajectories taken at a temperature of 8 GK, is shown by the yellow histogram. We refer to the Supplementary Text for more details.

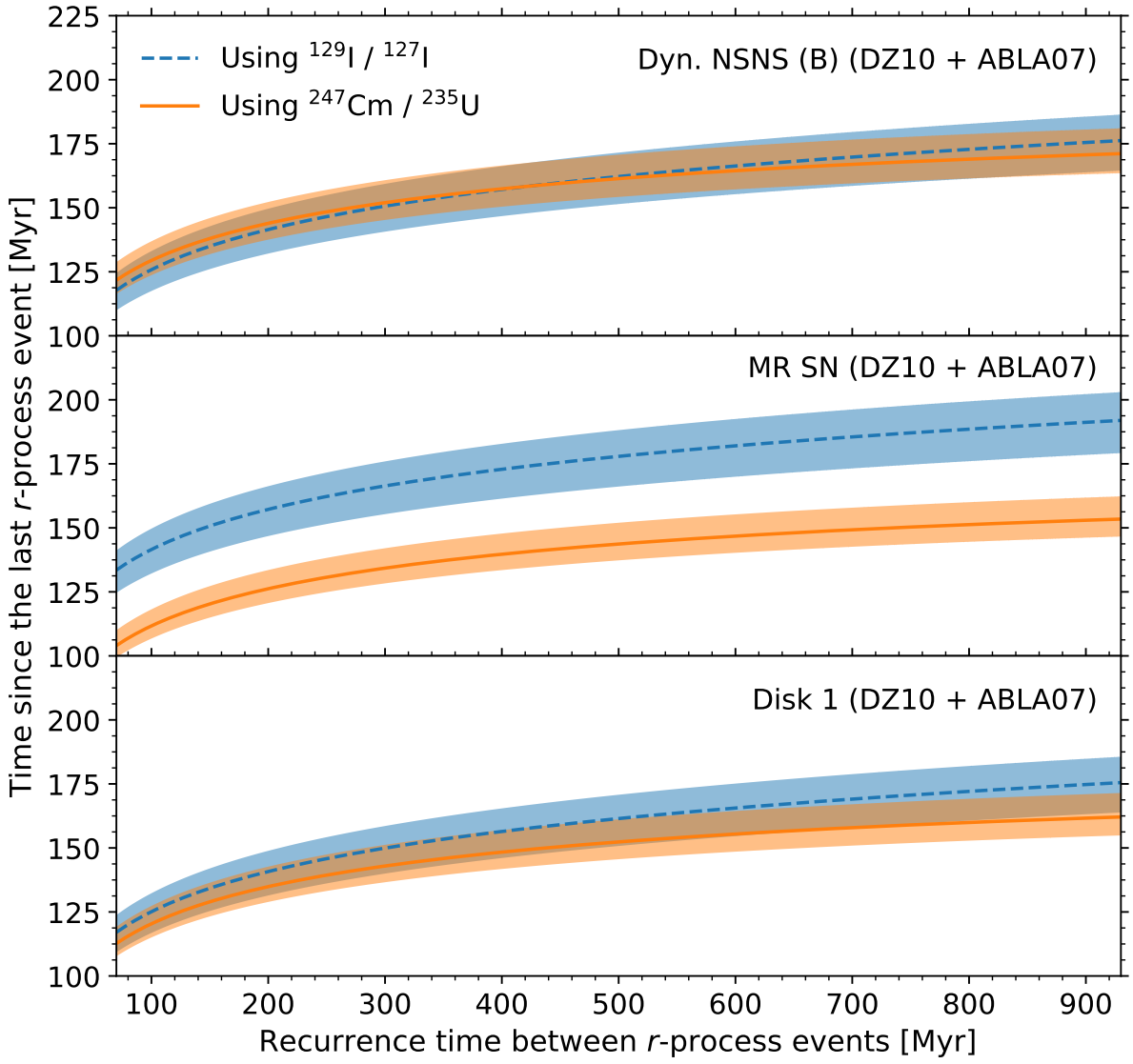

Fig. S3. Time Δt_{LE} elapsed between the last r-process event and the formation of the first solids in the early Solar System, using different nucleosynthesis models (different panels) to generate the last r-process enrichment of the pre-solar nebula. The dashed and solid lines show our predictions using the abundances of ^{129}I and ^{247}Cm, respectively, as independent tracers of that time. The uncertainty bands surrounding each line represent the 2σ uncertainty due to uncertainties in the half-life of ^{129}I and ^{247}Cm. We refer to the Supplementary Text for more details.

Label	Type of scenario	Setup	Reference	Name in reference
NSNS (R)	NSNS merger dynamical ejecta	1.0 $M_\odot$ + 1.0 $M_\odot$, Shen EOS	[20–22]	Run 1
NSBH (R)	NSBH merger dynamical ejecta	1.4 $M_\odot$ + 5.0 $M_\odot$, Shen EOS	[20–22]	Run 22
NSNS (B)	NSNS merger dynamical ejecta	1.25 $M_\odot$ + 1.25 $M_\odot$, SFHO EOS	[23]	SFHO-M1.25
MR SN	Magneto-rotational supernova	15 $M_\odot$, $B_0 = 5 \times 10^{12}$ G	[26]	w/ ν heating
Disk 1	NSNS merger disk ejecta	0.03 $M_\odot$ + 3.0 $M_\odot$, $s_0 = 8\ k_B/\mathrm{b}$, $\alpha = 0.03$	[24, 25]	S-def
Disk 2	NSNS merger disk ejecta	0.03 $M_\odot$ + 3.0 $M_\odot$, $s_0 = 6\ k_B/\mathrm{b}$, $\alpha = 0.03$	[24, 25]	s6
Disk 3	NSNS merger disk ejecta	0.03 $M_\odot$ + 3.0 $M_\odot$, $s_0 = 8\ k_B/\mathrm{b}$, $\alpha = 0.10$	[24, 25]	α0.10

Table S1. Description of the hydrodynamical models of r-process scenarios shown in Figs. 2 and S1. The labels in the first column correspond to the model labels found in those two figures. The setup column contains information on the the initial parameters of the simulations: masses and equation of state (EOS) for binary mergers; progenitor mass and initial magnetic field strength B_0 for the magneto-rotational supernova; torus and BH mass, initial entropy s_0 and viscosity parameter α for the disk scenarios.

NSNS merger scenario	Mass model	^{129}I / ^{247}Cm Range	^{129}I / ^{247}Cm Weighted average
NS1.2 - NS1.4	TF (D3C*)	$113.82 - 615.01$	360.69
	ETFSI-Q	$42.21 - 127.57$	92.29
	ETFSI	$37.94 - 108.56$	80.04
	FRDM2012 (D3C*)	$9.01 - 98.78$	67.19
	ETFSI (D3C*)	$3.55 - 126.40$	54.01
	SLY4	$8.79 - 37.31$	28.62
	TF	$11.77 - 25.74$	21.79
	HFB-17 (D3C*)	$2.34 - 36.20$	16.20
	FRDM2012	$5.10 - 23.69$	13.72
	UNEDF0	$8.28 - 17.50$	13.72
	HFB-21	$4.99 - 16.05$	9.24
	HFB-17	$6.18 - 13.21$	9.11
	DZ33	$5.16 - 8.74$	6.43
	FRDM1995	$2.44 - 8.31$	5.52
NS1.4 - NS1.4	TF (D3C*)	$223.93 - 599.49$	387.29
	ETFSI	$58.71 - 86.03$	69.06
	ETFSI-Q	$53.62 - 83.21$	67.60
	FRDM2012 (D3C*)	$15.72 - 89.16$	50.14
	ETFSI (D3C*)	$7.55 - 109.17$	38.91
	SLY4	$15.37 - 33.35$	27.18
	TF	$15.22 - 23.36$	19.83
	FRDM2012	$11.39 - 28.60$	16.65
	HFB-21	$6.82 - 15.45$	12.18
	UNEDF0	$11.19 - 13.06$	11.97
	HFB-17 (D3C*)	$2.66 - 30.54$	10.83
	HFB-17	$8.45 - 10.73$	9.33
	DZ33	$6.09 - 8.58$	7.40
	FRDM1995	$2.46 - 7.48$	4.33

Table S2. The ^{129}I / ^{247}Cm ratio predicted by PRISM network calculations using different mass models given the NSNS merger dynamical ejecta simulations from Refs. [20–22]. When labeled (D3C*), we used the Marketin β-decay rates [38], otherwise we used the Möller QRPA β-decay rates [55]. The numbers in the first column refer to the mass of the neutron stars in units of solar masses. The third column shows the range covered by all trajectories, while the fourth column shows the mass weighted average of those trajectories.

NSBH merger scenario	Mass model	^{129}I / ^{247}Cm Range	^{129}I / ^{247}Cm Weighted average
NS1.4 - BH5	TF (D3C*)	$123.91 - 231.83$	187.56
	ETFSI	$43.92 - 282.60$	83.01
	ETFSI-Q	$41.04 - 321.49$	81.59
	SLY4	$10.07 - 22.15$	14.94
	TF	$12.15 - 15.61$	13.80
	FRDM2012 (D3C*)	$8.65 - 15.61$	13.16
	UNEDF0	$8.43 - 14.01$	10.92
	HFB-21	$5.30 - 14.05$	10.43
	HFB-17	$7.39 - 22.95$	10.19
	FRDM2012	$5.37 - 13.43$	9.27
	DZ33	$5.20 - 13.11$	7.05
	ETFSI (D3C*)	$3.70 - 8.71$	6.02
	HFB-17 (D3C*)	$2.52 - 5.04$	3.45
	FRDM1995	$2.31 - 17.19$	3.42
NS1.4 - BH10	TF (D3C*)	$143.51 - 531.01$	235.37
	ETFSI-Q	$39.80 - 567.25$	84.49
	ETFSI	$38.39 - 73.23$	61.19
	FRDM2012 (D3C*)	$9.15 - 88.10$	23.80
	SLY4	$12.37 - 105.77$	23.33
	ETFSI (D3C*)	$3.96 - 116.48$	17.82
	TF	$11.51 - 21.94$	15.48
	FRDM2012	$7.92 - 17.66$	12.17
	HFB-21	$6.49 - 15.33$	11.55
	UNEDF0	$6.52 - 15.29$	11.27
	HFB-17	$8.00 - 14.37$	9.75
	DZ33	$4.63 - 13.39$	7.44
	HFB-17 (D3C*)	$2.47 - 32.40$	6.38
	FRDM1995	$2.47 - 36.30$	4.97

Table S3. Same as Table S2, but for NSBH mergers.

Type of successful scenario	**Occurrence probability**	**One event contributing to more than 90%**	**One event contributing to more than 99%**
Two disks	$33-40\%$	–	–
One disk	$66-54\%$	$98-84\%$	$95-51\%$
No disk	$1-6\%$	–	–

Table S4. Probability for two r-process events to combine their ejecta and generate a mixture consistent with the meteoritic ^{129}I/^{247}Cm ratio. In each cell, the two percentages correspond to the minimum and maximum cases described in the Supplementary Text. *Two disks*, *One disk*, and *No disk* refer to the number of disk event(s) among the two r-process events. The third and fourth columns show the probability that a single disk event contributed to more than 90% and 99% of the amount of both ^{129}I and ^{247}Cm in the early Solar System. Such probabilities are not meaningful for the *Two disks* scenario because in our experiment the nucleosynthesis products were the same for both disks. For the *No disk* scenario, the two events individually did not have an ^{129}I/^{247}Cm ratio consistent with the meteoritic ratio.